Flow Diagnostics for Optimal Polymer Injection Strategies

Stein Krogstad
SINTEF ICT

Knut-Andreas Lie
SINTEF ICT

Halvor Møll Nilsen
SINTEF ICT

Carl Fredrik Berg
Statoil

Vegard Kippe
Statoil

August 2, 2016

Abstract

This work extends the applicability of a class of flow-diagnostic computational tools for interactive visualization and fast simulation approximations to also account for polymer mobility effects. Flow diagnostics, as used here, employ simplifications to the reservoir flow equations to enable computation of quantitative (and detailed) information about the flow behavior of full 3D reservoir models within a few seconds.

Previously, we have utilized a linearized pressure equation and a corresponding set of time-of-flight (TOF) and stationary tracer equations to compute dynamic heterogeneity measures that correlate well with oil recovery for waterflooding scenarios. To also approximate the macroscopic effect of EOR injection strategies, we suggest an implicit approach for flow diagnostics in which polymer mobility effects are included approximately in the flow equation by linearizing the flux functions. Although this linearization has a pronounced smearing effect on the water and polymer fronts, we show that the heterogeneity of the total flux field is adequately represented. Subsequently we (re)solve the transport equations accurately along a 1D TOF-grid for each well-pair region. A recovery proxy is then obtained by accumulating each 1D solution weighted by a corresponding total TOF-distribution function.

We apply our new approach to 2D and 3D reservoir simulation models, and observe close agreements between the suggested single-step approximations and results obtained from full simulations. Furthermore, we demonstrate that explicit versus implicit versions of the proxy can be utilized to differentiate between macroscopic and microscopic sweep improvements resulting from polymer injection. For the examples considered, we demonstrate that macroscopic sweep improvements alone correlate better with measures for heterogeneity than the combined improvements.

Introduction

Modern reservoir simulators provide detailed forecasts of hydrocarbon recovery based on a description of reservoir geology, flow physics, well controls, and couplings to surface facilities. To interpret these simulations, it is common to study well profiles and 3D visualization of pressure, saturation, and component distributions in the reservoir. However, this is seldom sufficient to develop an understanding of how the reservoir reacts to changes in production strategies. A reservoir engineer will also want to know which injection and production wells are in communication; what is the sweep and displacement efficiency within a given drainage, sweep, or well-pair region; which regions of the reservoir are likely to remain unswept, and so on. Likewise, one must understand how different parameters in the reservoir model and their inherent sensitivity affect the recovery forecasts. Detailed simulations of field models take hours or days, and this limits the ability to iteratively perturb simulation input to evaluate and build *cause and effect* knowledge of the model. Rapid screening capability and simple, efficient, and interactive tools that can be used to develop basic understanding of how the fluid flow is affected by reservoir geology and how the flow patterns in the reservoir respond to engineering controls are needed to accelerate modelling workflows, make better use of time-consuming simulation runs, and provide better data for decision support.

The term *flow diagnostics*, as used here, are simple and controlled numerical flow experiments run to probe a reservoir model, establish connections and basic volume estimates, and quickly provide a qualitative picture of the flow patterns in the reservoir, either as a standalone prescreening tool or to post-process standard multiphase simulations (Shahvali et al., 2012; Møyner et al., 2014). Flow diagnostics can also be used to compute quantitative information about the recovery process in settings somewhat simpler than what would be encountered in an actual field, or be used to perform what-if and sensitivity analyzes in a parameter region surrounding a preexisting simulation. As such, these methods offer a computationally inexpensive alternative to the use of full-featured multiphase simulations to provide flow information in various reservoir management workflows.

Two types of information are fundamental in flow diagnostics: time-of-flight and volumetric (tracer) partitions. Time-of-flight τ denotes the time it takes a neutral particle to flow from the nearest inlet to a given point in the reservoir and defines natural time lines that describe how displacement fronts will propagate under prevailing flow conditions for an instantaneous flow field $\vec{v}$. Time-of-flight has traditionally been associated with streamline methods (Datta-Gupta and King, 2007; Thiele, 2005), but can equally well be computed by a finite-volume method (Natvig et al., 2006, 2007). Using a finite-volume formulation extends better to unstructured grids and provides more seamless integration with standard modelling tools currently used in industry. On differential form, τ is given as

$$\vec{v} \cdot \nabla \tau = \phi, \quad \tau|_{\text{inflow}} = 0, \tag{1}$$

where ϕ is the porosity of the reservoir. Volumetric partitions and measures of to what extent each cell in the reservoir is in communication with the different fluid sources and sinks can be determined by studying numerical tracers, which can be though of as artificial tracer injections continued until time infinity under steady flow conditions. Normalized tracer concentrations are given by simple advection equations on the form

$$\vec{v} \cdot \nabla c = 0, \quad c|_{\text{inflow}} = 1. \tag{2}$$

From time-of-flight and tracer distributions, one can derive various quantities that express volumetric connections and flow patterns such as drainage and sweep regions, well-pair connections and flow volumes, and well-allocation factors, which all are visually intuitive quantities giving enhanced understanding during pre- and post-processing (Møyner et al., 2014).

The ultimate goal of most reservoir simulation studies is to contribute to maximize profit given a set of operational and economic constraints. To this end, one need to explore various production strategies and perform a number of what-if and sensitivity analyzes. Sweep theory from classical reservoir engineering includes a number of heterogeneity measures for the variation in petrophysical properties like flow and storage capacity, the Lorenz and Dykstra–Parsons coefficients, etc. (Lake, 1989). It has been shown

that time-of-flight can be used to generalize this theory to a dynamic setting to provide measures of the heterogeneity in flow paths rather than in static reservoir properties. Heterogeneity measures like sweep efficiency, Lorenz coefficient, and vorticity index have proved to correlate well with recovery (Izgec et al., 2011; Rashid et al., 2012b; Møyner et al., 2014). These measures are all inexpensive to compute, and with a finite-volume formulation it is also straightforward to develop adjoint equations to compute gradients and parameter sensitivities which in turn can be utilized in effective optimization methods. In previous research (Møyner et al., 2014), we have used this idea to develop efficient workflows for optimizing well placement, drilling sequence, and production rates. We have also shown how effective proxies for economic objectives like net-present value can be derived from time-of-flight and tracer partitions, and how these in turn can be used to formulate highly efficient optimization loops for suggesting plausible sequences of rate targets which later can be slightly adjusted by a full-fledged simulation to derive production schedules that fulfill multiphase well constraints. Often, it is more difficult to formulate the objective and economic and engineering constraints in a precise mathematical form than solving the resulting problem. Exploring a large number of alternative formulations is usually prohibitive when relying on full-fledged multiphase simulators. Various forms of flow diagnostics, on the other hand, are inexpensive to compute and therefore ideal in the exploratory part of an optimization workflow.

The idea of using time-of-flight and tracer distributions to generate flow-based proxies for accelerating reservoir management workflows is not new. Diagnostic tools formulated on top of streamline simulation have been applied, e.g., in ranking and upscaling of geostatistical models (Idrobo et al., 2000; Ates et al., 2005), to optimize well rates in water-flooding (Thiele and Batycky, 2003; Park and Datta-Gupta, 2011; Izgec et al., 2011; Wen et al., 2014), for flood surveillance on a pattern-by-pattern basis (Batycky et al., 2008), and to optimize fracture stages and horizontal well completions in tight gas reservoirs (Sehbi et al., 2011).

Herein, we will discuss to what extent flow-diagnostic ideas developed for water-flooding scenarios can be extended to polymer flooding. To this end, we first discuss alternative ways of computing the distribution of time-of-flight and residence times (i.e., the time a neutral particle spends traveling from an inflow to an outflow point) that utilize ideas from tracer modelling (Shook and Forsmann, 2005; Huseby et al., 2012). Then, we move on to discuss how to forecast the macroscopic effect of polymer flooding and provide inexpensive forecasts of hydrocarbon recovery. Viscosity change due to polymer flooding improves both the microscopic and macroscopic sweep efficiency (Sorbie, 1991; Lake, 1989). Polymers increase the viscosity of the displacing fluid and hence increase the fractional flow of oil to the flow of the displacing fluid, which in turn improves the microscopic sweep efficiency (Pope, 1980). This effect is most pronounced when the waterflooding has an unfavorable mobility ratio. Polymers also improve the macroscopic sweep by reducing channeling through heterogeneous reservoirs and through viscous cross-flow between layers of different permeability (Clifford and Sorbie, 1985). Herein we will investigate polymer efficiency by comparing polymer flooding simulations to corresponding waterflooding scenarios. As numerical examples we apply both single layers from the SPE 10 model 2 (Christie et al., 2001) and the more complex Norne field model (IO Center, NTNU, 2012). By comparing an explicit proxy that only accounts for the improved microscopic sweep along streamlines with an implicit calculation that also accounts for macroscopic effects, we can distinguish the microscopic and macroscopic polymer effects. As the macroscopic effects are linked to viscous cross-flow and conformance, they are expected to correlate with heterogeneity measures (Zhou et al., 2015). Correlation with the Lorenz coefficient and the vorticity index (Rashid et al., 2012a) is explored for the models under consideration.

Time-of-flight and distributions of residence time

Time-of-flight can essentially be computed in three different ways for an instantaneous flow field $\vec{v}$. The most obvious approach is to simply trace streamlines and compute time-of-flight τ in a *pointwise sense* by integrating the interstitial velocity field along these streamlines (Datta-Gupta and King, 2007)

$$\frac{d\vec{x}}{ds} = \vec{v}(\vec{x}), \qquad \tau(r) = \int_0^r \frac{\phi(\vec{x}(s))}{|\vec{v}(\vec{x})|} ds. \tag{3}$$

Using streamlines to compute τ gives high pointwise accuracy. Unfortunately, it is not always straightforward to trace streamlines in complex reservoir grids that may have polyhedral cell geometries and all sorts of challenging degeneracies. In particular, it is challenging to reconstruct a consistent velocity field $\vec{v}$ from the numerical fluxes that are typically available from a finite-volume reservoir simulator, associate the correct flux to each flow path, etc. There are general and versatile methods available, see e.g., Klausen et al. (2012), but these are relatively expensive for large and complex geological models. Likewise, there are problems associated with distributing well fluxes to streamlines and ensuring mass conservation, see e.g., (Kippe et al., 2007).

Alternatively, one can use a finite-volume discretization of (1), which approximates the volume-averaged value of τ in each cell of the computational grid. Using a first-order finite-volume method with upwind evaluation of fluxes preserves the *causality* of the underlying continuous equation (1) (all information follows streamlines), and this ensures that the resulting linear system can be permuted to (block) triangular form by performing a topological sort of the grid cells. Hence, (1) can be solved very efficiently in $\mathcal{O}(n)$ operations for a grid with n cells, see Natvig et al. (2006, 2007); Møyner et al. (2014). This solution procedure is also possible if one uses a higher-order discontinuous Galerkin discretization.

To shed more light into the finite-volume approach and its potential limitations, let us consider a discrete incompressible flux field $\mathbf{v}$ and a grid cell i with total influx v_i. Moreover, let

$$\mathbf{A}\tau = \mathbf{V}_\phi \quad \text{and} \quad \mathbf{A}^T\mathbf{c}_{(i)} = \mathbf{e}_i v_i \tag{4}$$

be the discrete TOF equation and the *backward* tracer-equation, respectively, for the case where a tracer is injected in cell i and allowed to flow in the reverse direction of $\mathbf{v}$. Here, $\mathbf{V}_\phi$ is the vector of pore volumes and $\mathbf{e}_i$ is a unit vector equal one in cell i and zero elsewhere. For the TOF-value τ_i of cell i, we then have the following:

$$\tau_i = \mathbf{e}_i^T\mathbf{A}^{-1}\mathbf{V}_\phi = \frac{1}{v_i}\mathbf{c}_{(i)}^T\mathbf{V}_\phi. \tag{5}$$

Accordingly, τ_i equals the pore volume of the upstream region of cell i (i.e., the drainage region) divided by the flux. For a highly heterogeneous drainage region, this means that τ_i will be the average of a distribution of potentially large variance. This averaging introduces a systematic bias in dynamic heterogeneity measures, which may be acceptable in some applications and can be somewhat reduced by a higher-order spatial discretization (Rasmussen and Lie, 2014).

To provide EOR production forecasts, however, we need more accurate prediction of breakthrough time and production profiles. To this end, we consider the distribution of τ for each grid cell and in particular for cells containing production wells. At an outflow boundary, τ equals the *residence time*, i.e., the total time a neutral particle has spent traveling from the inflow to the outlet. Distributions of residence times are used e.g., in the study of chemical reactors and tracer tests (Shook and Forsmann, 2005; Huseby et al., 2012). Let $\vec{v}$ be an incompressible flux field in a 3D domain Ω with $\nabla\cdot v = 0$ inside the domain, $\vec{v}\cdot\vec{n} = q_i$ on the inlet boundary Γ_i and $\vec{v}\cdot\vec{n} = q_p$ on the outlet boundary Γ_p, and $\vec{v}\cdot\vec{n} = 0$ elsewhere on $\partial\Omega$. Consider the linear transport equation

$$\phi\frac{dc}{dt} + \vec{v}\cdot\nabla c(t) = 0, \quad c|_{\Gamma_i} = \delta(t), \tag{6}$$

with $c(x,0) = 0$. Thus, (6) describes the transport of a unit pulse through Ω. For each point x, the TOF-distribution p_x is simply the dirac function

$$p_x(t) = c(x,t) = \delta\big(t - \tau(x)\big), \tag{7}$$

while at the outlet, the (unit integral) TOF/residence-time distribution is given as

$$p(t) = \frac{\int_{\Gamma_p} c(t)\vec{v}\cdot\vec{n}\,ds}{\int_{\Gamma_p}\vec{v}\cdot\vec{n}\,ds}. \tag{8}$$

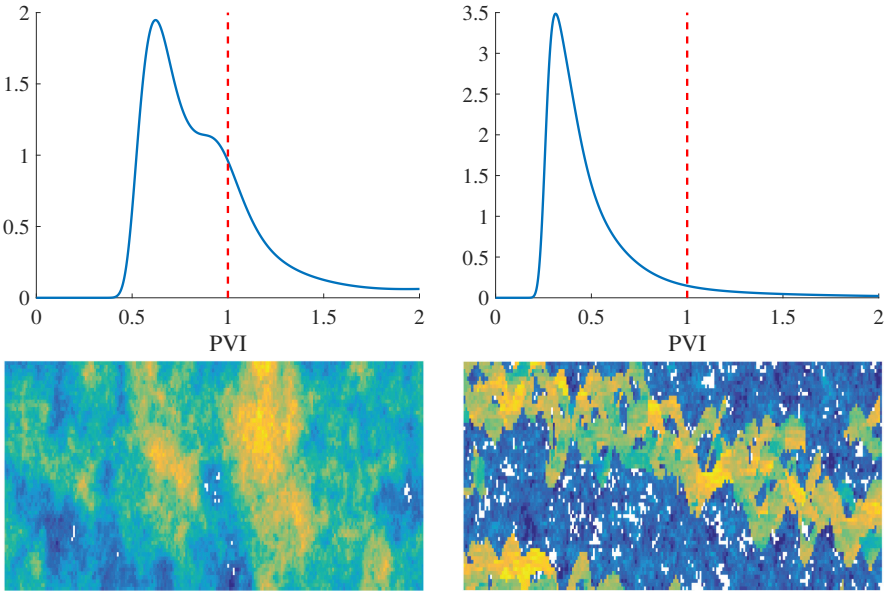

Figure 1 *Residence-time distributions for two different permeability fields in a left-to-right displacement scenario. Note that the mean of the distributions (dashed red line) equals* 1 *PVI (pore volume injected).*

To see the connection between (1) and (6), we consider the first-order moment $m_1 = \int_0^\infty tc\,dt$, which can be obtained by multiplying (6) with t and taking the integral

$$\int_0^\infty \left[\phi \frac{dc}{dt} t + \vec{v}\cdot\nabla(tc(t))\right] dt = \phi\left([tc]_{t=0}^\infty - m_0\right) + \vec{v}\cdot\nabla(m_1) = 0. \tag{9}$$

This equation simplifies to

$$\vec{v}\cdot\nabla m_1 = \phi, \quad m_1|_{\Gamma_i} = 0, \tag{10}$$

since $m_0 = \int_0^\infty c\,dt = 1$ and $\lim_{t\to\infty} c(t) = 0$. Accordingly, m_1 equals τ as defined by (1). Equation (10) is the first of a family of moment equations Leube et al. (2012), for which the higher-order (raw) moments can be computed according to

$$\vec{v}\cdot\nabla m_k = k\,\phi\,m_{k-1}, \quad m_k|_{\Gamma_i} = 0. \tag{11}$$

Note that by (7), for any point x, $m_k(x) = 0$ for $k \geq 2$, while this is not the case for residence time distributions of the form (8).

Discretized equations for TOF/residence-time distributions

Analogous to (6), we may write the semi-discrete pulse-equation as a linear set of ODEs of the form

$$\frac{d\mathbf{c}}{dt} + \mathbf{M}\mathbf{c} = 0, \quad \mathbf{c}(0) = \mathbf{c}_0 = \frac{\mathbf{q}_i}{\mathbf{V}_\phi}, \tag{12}$$

where $\mathbf{M}$ is a discretization of the linear operator $\frac{1}{\phi}\vec{v}\cdot\nabla$ and $\mathbf{q}_i$ is the vector of injection source terms. The discrete linear operator $\mathbf{M}$ is constructed using the standard upwind scheme (as is common in most finite-volume based reservoir simulators). The solution of (12) is given in terms of matrix exponential by $\mathbf{c}(t) = e^{-t\mathbf{M}}\mathbf{c}_0$. Hence, the discrete counterparts of (7)–(8) can be represented by

$$p_i(t) = \mathbf{e}_i^T e^{-t\mathbf{M}}\mathbf{c}_0 \quad \text{and} \quad p_w(t) = \mathbf{q}_w^T e^{-t\mathbf{M}}\mathbf{c}_0 / \mathbf{q}_w^T\mathbf{e}, \tag{13}$$

respectively, where $\mathbf{q}_w$ is the vector of source terms in the producers (or fluid sinks) and $\mathbf{e}$ is the vector of ones. In Figure 1, two residence-time distributions are depicted for two permeability fields with distinctly different heterogeneity. The channelized field is seen to naturally have a sharp peak far left of the mean.

Analogous to (11), the moments $m_{w,k}$ of $p_w(t)$ for $k \geq 1$ can be obtained by

$$m_{w,k} = \frac{\mathbf{q}_p^T \mathbf{m}_k}{\mathbf{q}_p^T \mathbf{e}}, \quad \mathbf{M}\mathbf{m}_k = k\,\mathbf{m}_{k-1}, \tag{14}$$

with $\mathbf{m}_0 = \mathbf{e}$. We note that, given a residence time distribution $p_w(t)$, the flow capacity and storage capacity curves are simply given as (Shook and Forsmann, 2005)

$$F(t) = \int_0^t p_w(s)\,ds, \qquad \Phi(t) = \int_0^t s\,p_w(s)\,ds. \tag{15}$$

For efficient computation of residence-time distributions we employ a rational Padé approximation to evaluate the action of the matrix exponential, i.e.,

$$p(t+\Delta t) = e^{-\Delta t M} p(t) \approx P(-\Delta t M)\,Q(-\Delta t M)^{-1} p(t), \tag{16}$$

for suitable polynomials P and Q. Herein, we use first-order polynomials to reduce fill-in, i.e., $P(x) = 1 + x/2$ and $Q(x) = 1 - x/2$. Accordingly, for each successive value of the distribution we compute, we need to solve a linear system. However, for the problems we consider, the matrix $\mathbf{M}$ is triangular possibly after permutation (Natvig et al., 2007), and hence each linear solve is highly efficient. We note that an alternative approach is to solve the *truncated moment problem*, i.e., to compute the first n moments of the distribution from (11), and then try to find a distribution sharing the same moments. One approach towards this is the *maximum entropy method* (see e.g., Mead and Papanicolaou (1984)), which involves solving a set of n non-linear equations. In our initial tests, however, we found that obtaining convergence for these equations could be difficult, especially for distributions with long, slim tails towards infinity. This is typically the case for residence-time distributions from highly heterogeneous permeability fields like the one shown to the right in Figure 1.

A recovery proxy for polymer flooding

In the following, we will use the residence-time distribution to develop a proxy for evaluating the performance of polymer flooding. The word 'proxy' is often used to denote response surface models derived from a series of full flow simulations. Herein, we will use the same word to denote a reduced model with simplified flow physics that can approximate recovery curves.

To describe polymer flooding, we consider an immiscible, two-phase model with three fluid components (oil, water, and polymer) on the form,

$$\begin{aligned} \partial_t(\phi b_o s_o) + \nabla\cdot(b_o \vec{v}_o) - b_o q_o = 0, \qquad & \vec{v}_o = -\lambda_o K(\nabla p_o - \rho_o g \nabla z) \\ \partial_t(\phi b_w s_w) + \nabla\cdot(b_w \vec{v}_w) - b_w q_w = 0, \qquad & \vec{v}_w = -\lambda_w K(\nabla p_w - \rho_w g \nabla z) \\ \partial_t(\phi_{dpv} b_w s_w c_p) + \partial_t(\rho_r c_a(1-\phi_r)) + \nabla\cdot(b_w c_p v_p) - b_w q_p = 0, \qquad & \vec{v}_p = -\lambda_p K(\nabla p_w - \rho_w g \nabla z). \end{aligned} \tag{17}$$

This model is sufficiently general to incorporate most of the fluid effects found in commercial simulators, like adsorption of polymer onto the reservoir rock, reduction in permeability, inaccessible pore space, mixing of polymer in water, compressibility of fluids and rock, as well as pseudoplastic effects of the diluted polymer solution. As our multiphase reference, we will use an open-source simulator (Hilden et al., 2016) that includes all these effects.

Capturing macroscopic sweep effects in a single step

The first goal of the current flow-diagnostics approach is to efficiently obtain a flux field taking into account changing mobility effects originating from injection of polymer. Omitting adsorption, compressibility, dead pore space, gravity, and pseudoplastic effects, (17) can be written in total flux form:

$$\begin{aligned} \vec{v} = -(\lambda_w + \lambda_o)\mathbf{K}\nabla p, \quad \nabla\vec{v} = q, \\ \partial_t(\phi s_w) + \nabla\cdot(\vec{v} f_w) = q_w, \qquad \partial_t(\phi s_w c_p) + \nabla\cdot(\vec{v} f_p c_p) = q_w c_{\text{inj}}, \end{aligned} \tag{18}$$

where $\vec{v} = \vec{v}_w + \vec{v}_o$, $f_w = \lambda_w/(\lambda_w + \lambda_o)$ and $f_p = \lambda_p/(\lambda_w + \lambda_o)$. Although the equations in (18) are greatly simplified compared to (17), they are still highly nonlinear, and obtaining a flux field $\vec{v}$ at some finite end time T requires a simulation. To be able to compute this solution within a single time-step $\Delta t = T$, we linearize f_w and f_p between their endpoints. The fully-coupled system is still nonlinear, but using linear flux functions improves the convergence of the Newton solver used to solve the nonlinear system. (Using a trust-region solver, e.g., as discussed by Møyner (2016), could be an alternative to linearization of the flux functions, but such solvers have not yet been developed for polymer flooding.) Obviously, taking extremely long time steps like this will lead to severe smearing of the saturation and concentration fronts, and hence the solution cannot be used to predict fluid production. However, in the next step of the proxy, we reevaluate the saturation front based on the residence-time distributions for the flux field $\vec{v}$ obtained from (18).

Mapping 1D displacement fronts to residence time distributions

In the second part of the proxy, we partition the flux field in injector–producer interaction regions, and solve representative 1D transport problems along τ for each region. The interaction regions are obtained by solving (forward and backward) stationary tracer equations, see Møyner et al. (2014) for details. For each interaction region, we then perform the following three steps:

1. Compute the TOF/residence-time distribution for the region.
2. Map the saturation/concentration fields of the region onto a 1D TOF-grid ($s_0(\tau)$) using a suitable averaging procedure, and run a 1D simulation on the grid from time zero to horizon T. As a result, we get the saturation changes as a function of τ, i.e., $\Delta s(\tau) = s(\tau) - s_0(\tau)$.
3. Estimate the total volume of produced oil for the region by integrating the product of the residence-time distribution and cumulative volume of additional water along τ. That is, the produced volume of oil r_o from time 0 to time T for the region is estimated as

$$r_o = \int_0^\infty p(\tau) \int_0^\tau \Delta s(\tilde{\tau})\, d\tilde{\tau}\, d\tau. \tag{19}$$

The overall procedure is illustrated in Figure 2 and has obvious similarities with streamline simulation (think of each region as a bundle of streamlines). If necessary, the proxy can be refined by computing the volumetric partition based on well segments instead of individual wells.

Numerical examples

To validate the practical usefulness of flow diagnostics for EOR, the methods introduced above were implemented as an enhancement to the `diagnostics` module from the open-source Matlab Reservoir Simulation Toolbox (MRST, 2015b; Lie, 2015).

Horizontal layers from SPE 10

In our first numerical example, we consider the horizontal layers of the synthetic Brent model used in the 10th SPE Comparative Solution Project (Christie et al., 2001). The full model consists of a grid with $60 \times 220 \times 85$ cells, where the top 35 layers represent the shallow-marine Tarbert formation, which has a log-normal permeability distribution, while the lower 50 layers represent the fluvial Upper Ness formation with distinct permeability distributions for the high-permeable channels and the lower-permeable background. We consider a scenario with a single injector and a single producer, each well perforating an entire side of the model (see Figure 3). The injector is controlled by a constant rate, while the producer is controlled by a constant pressure. The reference simulations are run as follows

1. From $t_0 = 0$, inject water only until the water cut in the producer reaches 0.9 (t_1).
2. From t_1, inject water with a polymer concentration $1 kg/m^3$ until a total of $51\,000 kg$ polymer has been injected. For most layers this amounts to approximately 0.8 PVI (t_2). For comparison, we also simulate $[t_1, t_2]$ injecting water only.

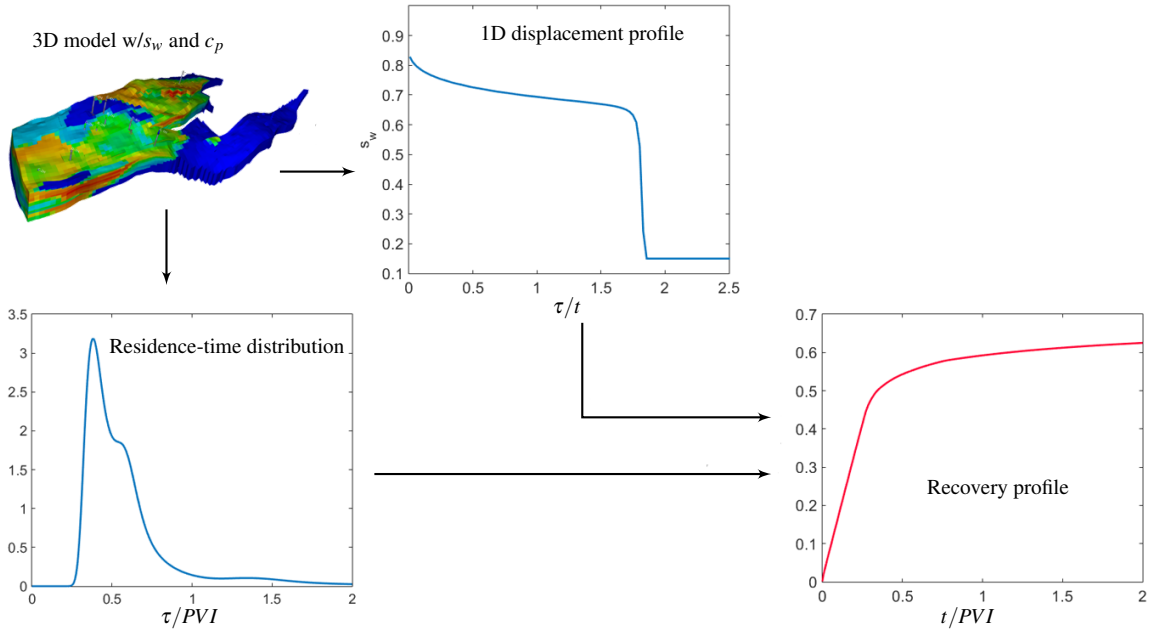

Figure 2 *Illustration of the recovery proxy. The reservoir is partitioned into injector–producer regions. Then, residence-time distributions and representative 1D displacement profiles are computed for each region and convolved to compute the recovery proxy.*

The middle and right plots in Figure 3 show the reference solution with and without polymer depicted as solid and dashed lines, respectively, for one layer in each of the two different formations. Next, we evaluate the proxy for all layers. For comparison and subsequent approximation of macroscopic versus microscopic sweep improvements, we compute both an implicit (as previously described) and an explicit version of the proxy. For the explicit version, we simply solve (18) with a zero time step, e.g., solve a pressure equation based on the current state. Then, the flow pattern will be locked to the current state, and not represent changes in streamlines due to mobility changes. This way, the explicit version will only include the effect of improved microscopic sweep due to changes in fractional flow and not reflect improved macroscopic sweep. We note that for evaluation purposes, results from the explicit proxy were compared to results from a sequential simulator which was modified to use fixed velocity for all time steps. This comparison (not reported here) showed close agreement between the proxy and modified simulation. The proxies are run as follows:

1. For the first period $[0,t_1]$, we evaluate the explicit and implicit proxies for various time horizons $T <= t_1$.
2. For the second period $[t_1,t_2]$, we evaluate the explicit and implicit proxies for various time horizons $T <= t_2 - t_1$ both with and without polymer injection.

Figure 3 shows the proxy predictions for Layers 23 and 75 for the first period (water only) and for the second period (polymer or water only). As observed, there is little difference between explicit and implicit during the first period, while for the polymer injection in the second period, the two proxies differ substantially for the highly heterogeneous Upper Ness case (Layer 75), but only marginally for the more homogeneous Tarbert case (Layer 23). This indicates that the recovery increase due to polymer for Layer 23 is mainly due to microscopic sweep improvements, while for Layer 75 macroscopic sweep improvement is dominating.

Figure 4 shows the correlation for all layers between recovery factors computed by the proxies and reference recovery factors obtained from full simulations. The upper row shows all proxy evaluations for the water-flooding scenario. For the first period (upper right), a (slight) bias is observed for the longer time steps. Note however, that the reservoir is almost completely flooded during this period (water cut

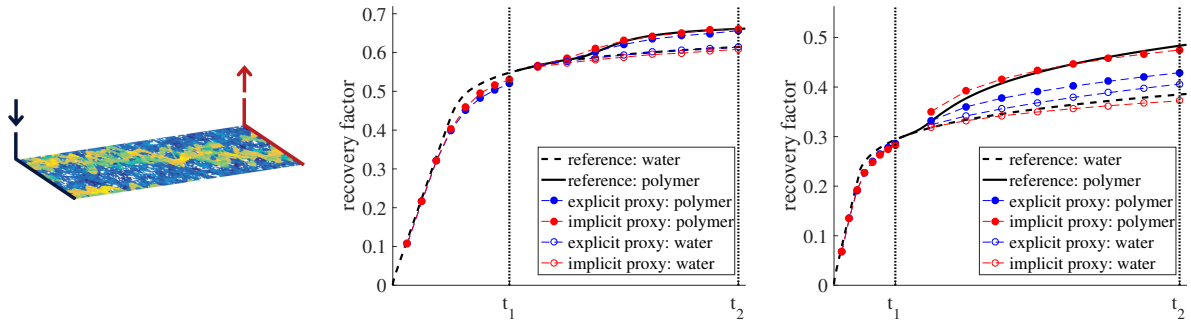

Figure 3 *Well setup for each layer of the SPE10 model (left), and reference and proxy output for Layer 23 (middle) and Layer 75 (right). Dashed black line is reference recovery factor without polymer injection, solid black line is reference recovery for polymer injection starting at t_1 (water cut 0.9). Red dots (polymer injection) and circles (water injection) show proxy predictions for various time horizons using the implicit proxy, while blue dots and circles correspond to explicit proxy.*

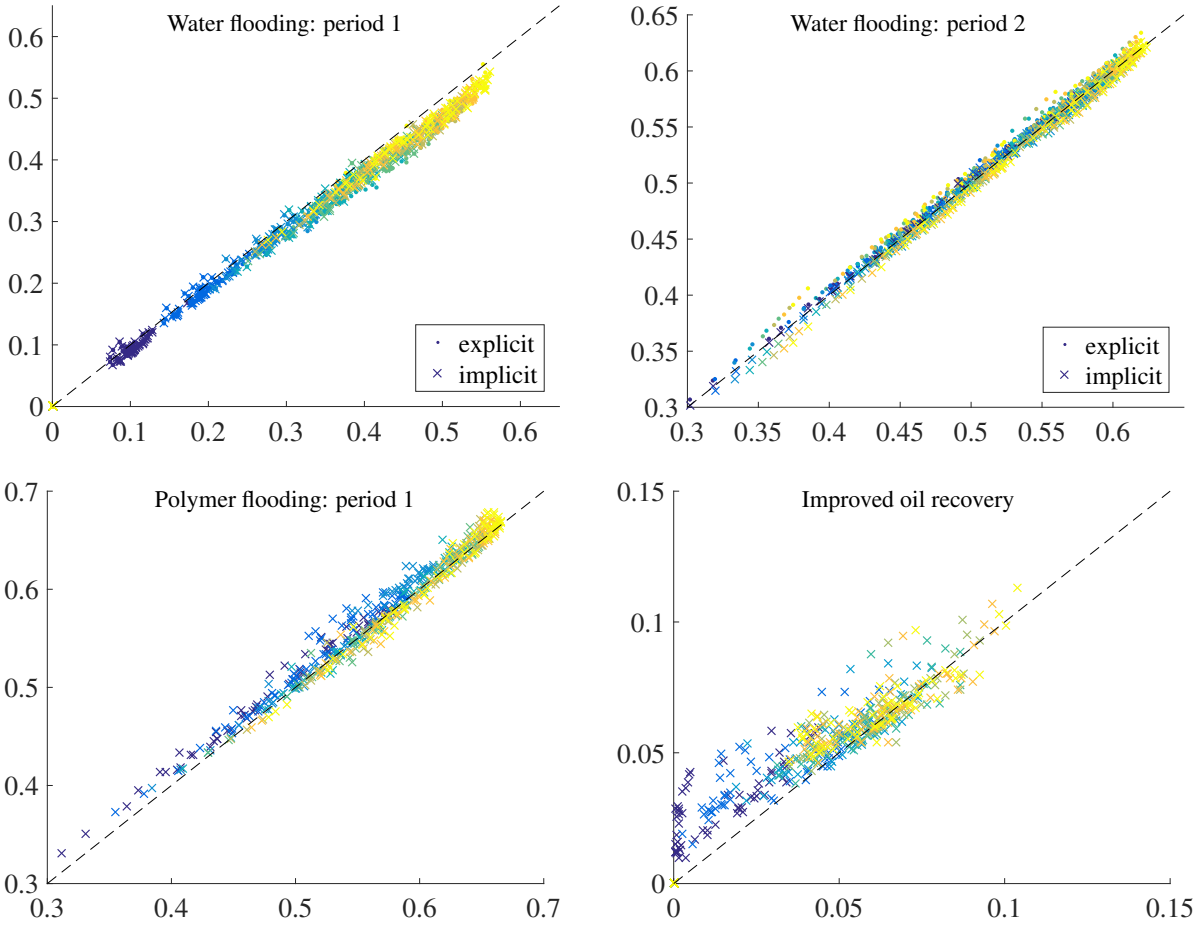

Figure 4 *Correlation betwen recovery predicted by the proxy (y-axis) and by a full simulation (x-axis) for all horizontal layers of the SPE 10 model. The proxy is run with different time-step sizes, varying from short (blue) to the whole period (yellow).*

from zero to 0.9), so some discrepancies are expected. For the second period (upper left), the proxy predictions are very well correlated with the reference. Note also that there are no significant differences between the explicit and implicit proxies for these cases. In the lower-left plot, all implicit proxy evaluations for the polymer injection case are plotted versus reference values from full simulations. In this case, the explicit proxy evaluations are omitted as they fail to give adequate predictions. Although the implicit proxy correlates well with a full multiphase simulation, it has a tendency to overpredict recovery for the shorter time steps (prior to polymer breakthrough). This effect becomes more pronounced when we plot the predicted increase in oil recovery due to polymer, i.e., recovery from polymer injection minus recovery from water only (lower-right plot).

Finally, we wish to isolate the macroscopic and microscopic sweep improvements by comparing the implicit and explicit proxies. Since a standard simulator cannot give predictions of these quantities, we rather compare them with measures of heterogeneity, i.e., the Lorenz coefficient and the vorticity index. As above, we estimate the improvement in total recovery by comparing the implicit proxy for polymer injection to the implicit proxy for pure water injection. We estimate the improved recovery due to microscopic effects by comparing the explicit proxy for polymer injection to the implicit proxy for pure water injection. And finally, we estimate the improved recovery due to macroscopic effect as the difference between total improved recovery and recovery improved by microscopic effects. Figure 5 depicts the resulting improved recoveries for all layers. As expected, there is no apparent correlation between heterogeneity and microscopic sweep improvements. The best correlation (for both measures) is observed between heterogeneity and macroscopic improvements. Accordingly, these results illustrate that the largest gain for polymer injection is obtained for high heterogeneity. We note that the line of best fit for macroscopic improvements versus Lorenz coefficient does not pass trough the origin, hence it appears that the relation is not linear even though they are strongly correlated.

The Norne field model

In this example we adapt a model of the Norne field (IO Center, NTNU (2012)), to test our suggested proxy in a realistic setting with multiple wells (see Figure 6). Again, we consider a two-phase oil/water model with subsequent polymer injection. Flow functions for water/oil/polymer are the same as in the previous example. In this example, the entire reservoir is initially at residual water saturation. Water is injected at constant rate for approximately 20 years, while producers are shut when a water-cut of 0.9 is reached. As a result, at the end of the first period, five of the nine producers have been closed due to excess water-cut. In the second period, all wells are opened, and set to produce at a constant liquid rate for about 40 years (about 0.8 PVI). As in the previous example, both pure water and polymer injection is considered. In the polymer case, all six injectors are set to inject a mixture of concentration $1 kg/m^3$. The implicit and explicit proxies are run for time horizons of $10, 20, 30$ and 40 years for both injection scenarios. With six injectors and nine producers, there are potentially 54 interaction regions. However, in the current scenarios there are 14 producer-injector pairs with zero or negligible communication, and hence TOF-distributions and 1D displacement profiles are computed for 40 regions for each proxy evaluation. In Figure 6 (right), the evolution of the overall recovery factor is shown. Similarly to the previous example, the proxy for polymer injection slightly overestimates the recovery for the shortest time horizon, but matches perfectly as the polymer mixture reaches most producers. We also observe a considerable difference in explicit versus implicit proxy, suggesting macroscopic sweep improvement due to polymer are present.

Since the proxy computes recovery for each (communicating) well-interaction region, we can also estimate recovery for each of the wells. Figure 7 reports cumulative recovery factors for four of the producers. For wells D-1CH and B-1BH, we observe that the polymer injection has a somewhat marginal effect, while the opposite is true for B-2H and D-2H. Note that the large improvements seen in these plots not only come from improved sweep in the drainage regions, but also from the fact that the drainage regions are enlarged.

Last, we look more closely at the recovery profile of producer B-2H (Figure 7, top-left) and decompose it according to the communicating injectors. The three injectors contributing most to production in B-2H

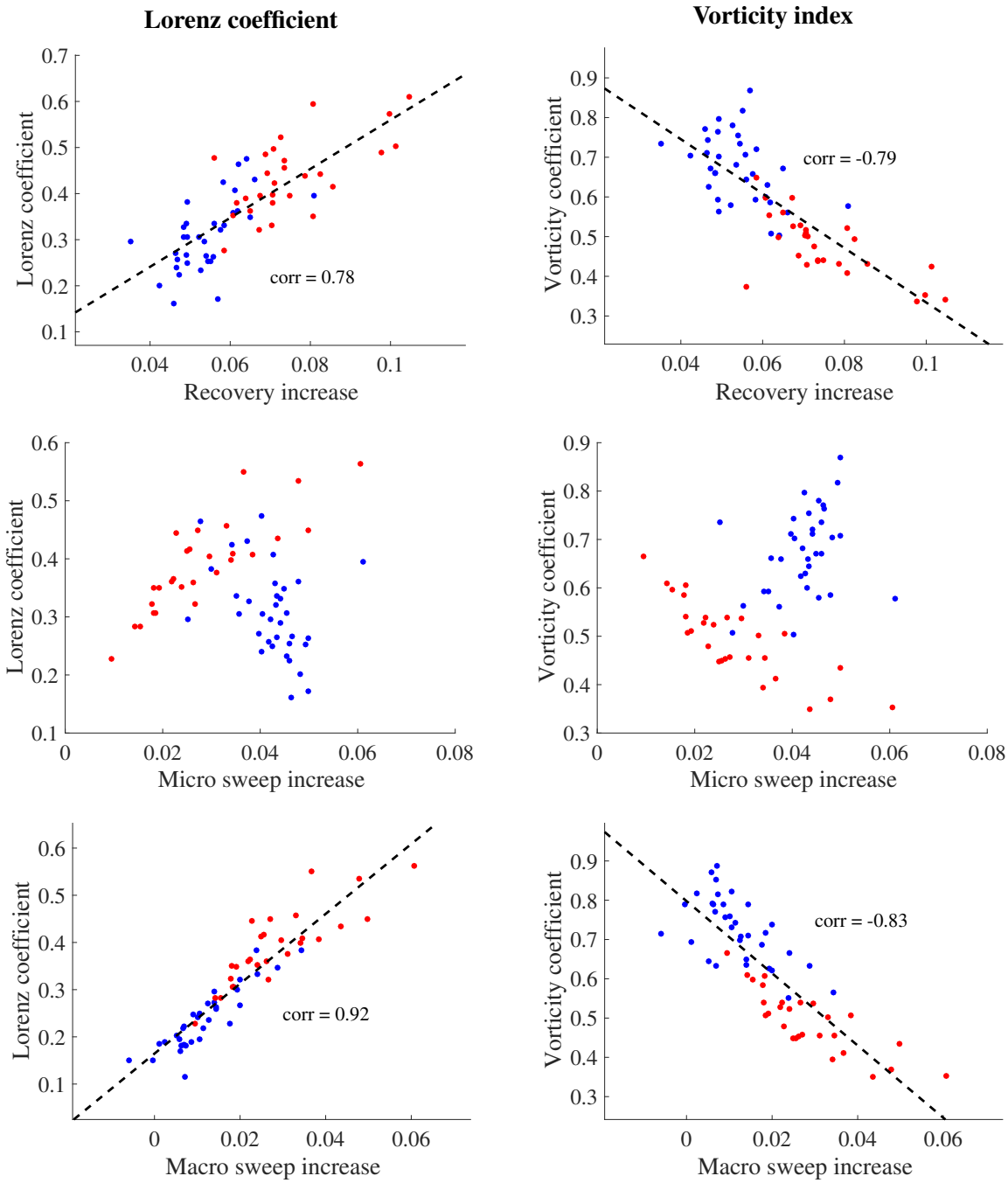

Figure 5 *Plot of heterogeneity measure (Lorenz coefficient or vorticity index) versus estimated increase in total (top), microscopic (middle), and marcroscopic (bottom) recovery due to polymer. Red dots correspond to the fluvial Upper Ness layers, blue to log-normal permeability fields of the Tarbert formation.*

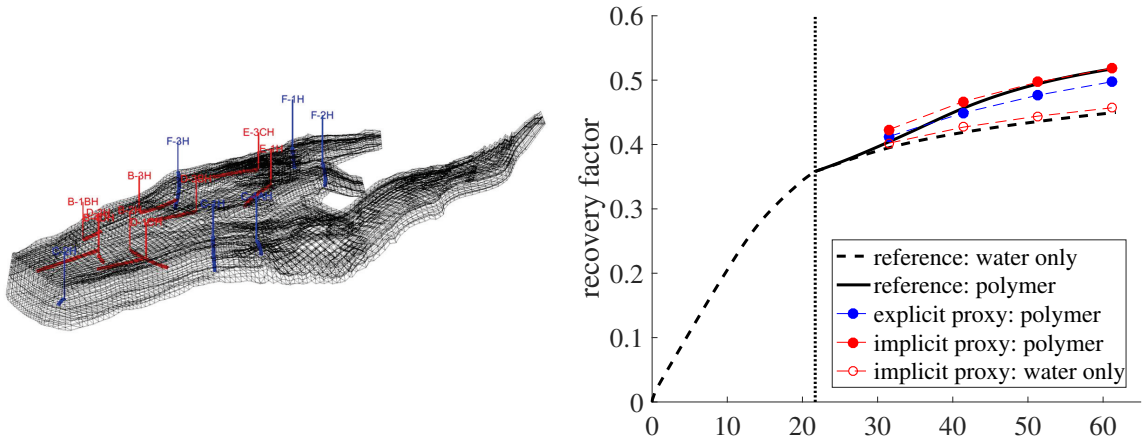

Figure 6 *Grid and well positions for the Norne model (left), and evolution of total field recovery factors from simulations and proxies (right).*

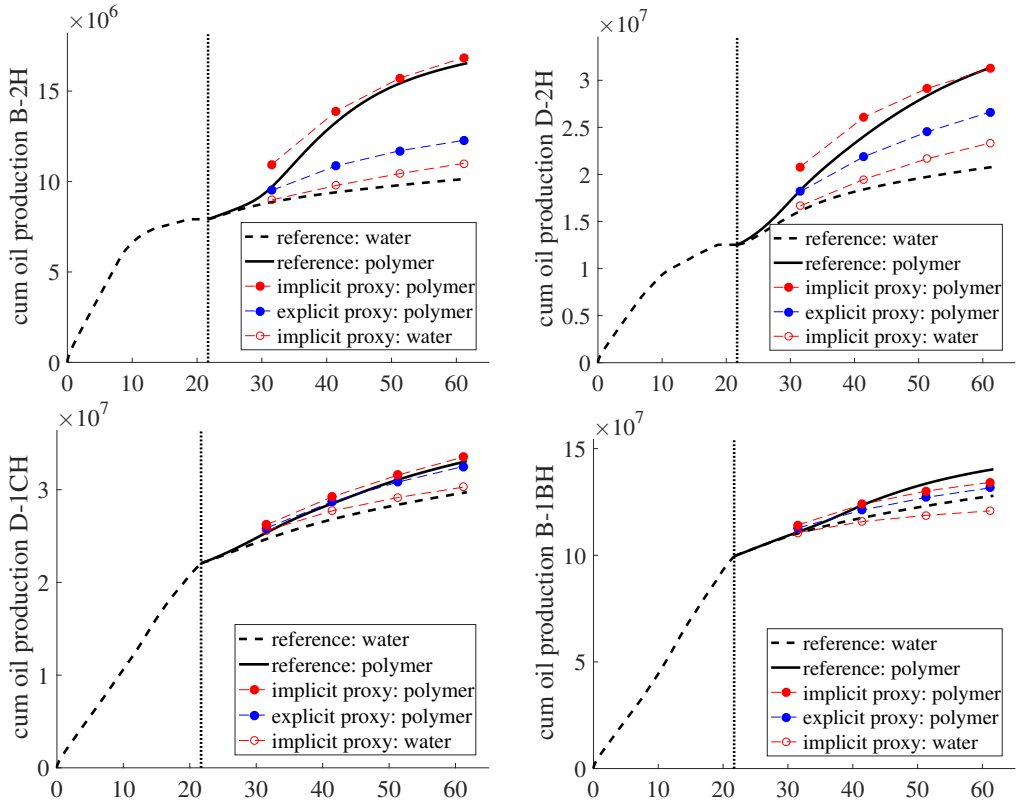

Figure 7 *Estimated evolution of recovery (simulation and proxy) for four of the producers.*

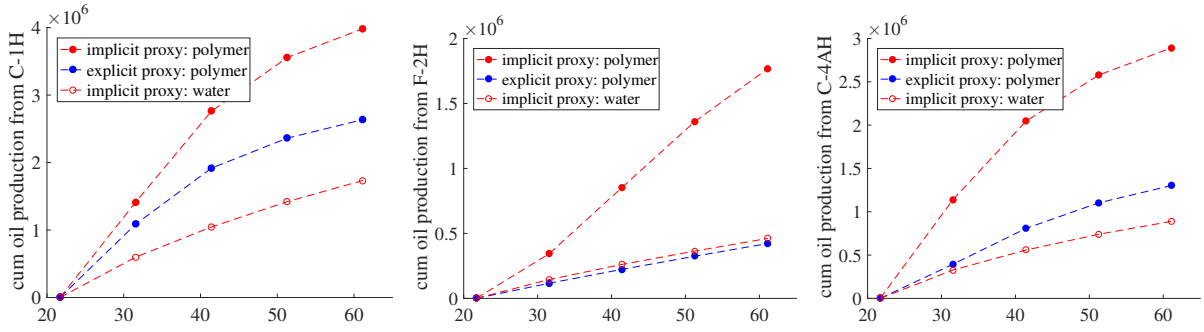

Figure 8 *Estimated evolution of partial recovery for producer B-2H from the three most contributing injectors.*

(measured in total flux) are C-1H, F-2H and C-4AH. Recovery plots for the corresponding interaction regions are shown in Figure 8. Since our multiphase simulator cannot provide us with recovery estimates broken down to individual well-pair regions, only the proxy-values for the second period are plotted. We observe that the polymer injection apparently has a large influence on the recovery from these regions.

Concluding remarks

We have presented a proxy for rapid evaluation of polymer injection scenarios in the framework of flow-diagnostics computational tools. Although taking inspiration from streamline methods, the proxy utilizes the same grid and discretization as a standard finite-volume based reservoir simulator. For the examples considered, the implicit versions of the proxy appeared to approximate both water and polymer flooding to a fair degree of accuracy. Thus it appears as a good candidate for optimization applications.

In addition, the explicit versus implicit versions of the proxy appeared to adequately differentiate between macroscopic and microscopic sweep improvements. This could be used to asses the impact of reservoir heterogeneity on polymer efficiency.

Acknowledgements

The authors wish to thank Statoil for partial funding of this work and for permission to publish the results. Also, we thank Statoil (operator of the Norne field) and its license partners ENI and Petoro for the release of the Norne data. Further, the authors acknowledge the IO Center at NTNU for coordination of the Norne cases.

References

Ates, H., Bahar, A., El-Abd, S., Charfeddine, M., Kelkar, M. and Datta-Gupta, A. [2005] Ranking and upscaling of geostatistical reservoir models using streamline simulation: A field case study. *SPE Res. Eval. Eng.*, **8**(1), 22–32.

Batycky, R.P., Thieles, M.R., Baker, R.O. and Chugh, S.H. [2008] Revisiting reservoir flood-surveillance methods using streamlines. *SPE Res. Eval. Eng.*, **11**(2), 387–394.

Christie, M.A., Blunt, M.J. and others [2001] Tenth SPE comparative solution project: A comparison of upscaling techniques. In: *SPE Reservoir Simulation Symposium*. Society of Petroleum Engineers.

Clifford, P.J. and Sorbie, K.S. [1985] The effects of chemical degradation on polymer flooding. In: *SPE Oilfield and Geothermal Chemistry Symposium*. Society of Petroleum Engineers.

Datta-Gupta, A. and King, M.J. [2007] *Streamline Simulation: Theory and Practice*, *SPE Textbook Series*, 11. Society of Petroleum Engineers.

Hilden, S.T., Møyner, O., Lie, K.A. and Bao, K. [2016] Multiscale simulation of polymer flooding with shear effects. *Transport in Porous Media*, **113**(1), 111–135.

Huseby, O., Sagen, J. and Dugstad, Ø. [2012] Single well chemical tracer tests – fast and accurate simulations. In: *SPE EOR Conference at Oil and Gas West Asia, Muscat, Oman, 16-18 April*.

Idrobo, E.A., Choudhary, M.K. and Datta-Gupta, A. [2000] Swept volume calculations and ranking of geostatistical reservoir models using streamline simulation. In: *SPE/AAPG Western Regional Meeting*. Long Beach, California, USA. SPE 62557.

IO Center, NTNU [2012] The Norne Benchmark Case. url: `http://www.ipt.ntnu.no/~norne/wiki/doku.php`.

Izgec, O., Sayarpour, M. and Shook, G.M. [2011] Maximizing volumetric sweep efficiency in waterfloods with hydrocarbon F-Φ curves. *J. Petrol. Sci. Eng.*, **78**(1), 54–64.

Kippe, V., Hægland, H. and Lie, K.A. [2007] A method to improve the mass-balance in streamline methods. In: *SPE Reservoir Simulation Symposium*. SPE 106250, Houston, Texas, U.S.A.

Klausen, R.A., Rasmussen, A.F. and Stephansen, A. [2012] Velocity interpolation and streamline tracing on irregular geometries. *Comput. Geosci.*, **16**, 261–276.

Lake, L.W. [1989] *Enhanced Oil Recovery*. Prentice-Hall.

Leube, P.C., Nowak, W. and Schneider, G. [2012] Temporal moments revisited: Why there is no better way for physically based model reduction in time. *Water Resour. Res*, **48**(11). W11527.

Lie, K.A. [2015] *An Introduction to reservoir simulation using MATLAB: User guide for the Matlab Reservoir Simulation Toolbox (MRST)*. SINTEF ICT, www.sintef.no/Projectweb/MRST/publications, 2nd edn.

Mead, L.R. and Papanicolaou, N. [1984] Maximum entropy in the problem of moments. *Journal of Mathematical Physics*, **25**(8), 2404–2417.

Møyner, O. [2016] Nonlinear solver for three-phase transport problems based on approximate trust regions. In: *ECMOR XV – 15th European Conference on the Mathematics of Oil Recovery*. EAGE, Amsterdam, The Netherlands.

Møyner, O., Krogstad, S. and Lie, K.A. [2014] The application of flow diagnostics for reservoir management. *SPE J.*, **20**(2), 306–323.

MRST [2015b] The MATLAB Reservoir Simulation Toolbox. www.sintef.no/MRST.

Natvig, J.R., Lie, K.A. and Eikemo, B. [2006] Fast solvers for flow in porous media based on discontinuous Galerkin methods and optimal reordering. In: Binning, P., Engesgaard, P., Dahle, H., Pinder, G. and Gray, W. (Eds.) *Proceedings of the XVI International Conference on Computational Methods in Water Resources*. Copenhagen, Denmark.

Natvig, J.R., Lie, K.A., Eikemo, B. and Berre, I. [2007] An efficient discontinuous Galerkin method for advective transport in porous media. *Adv. Water Resour.*, **30**(12), 2424–2438.

Park, H.Y. and Datta-Gupta, A. [2011] Reservoir management using streamline-based flood efficiency maps and application to rate optimization. In: *Proceedings of the SPE Western North American Region Meeting*. 7-11 May 2011, Anchorage, Alaska, USA.

Pope, G.A. [1980] The application of fractional flow theory to enhanced oil recovery. *Society of Petroleum Engineers Journal*, **20**(03), 191–205.

Rashid, B., Bal, A.L., Williams, G.J. and Muggeridge, A.H. [2012a] Using vorticity to quantify the relative importance of heterogeneity, viscosity ratio, gravity and diffusion on oil recovery. *Comput. Geosci.*, **16**(2), 409–422.

Rashid, B., Muggeridge, A., Bal, A.L. and Williams, G.J.J. [2012b] Quantifying the impact of permeability heterogeneity on secondary-recovery performance. *SPE J.*, **17**(2), 455–468.

Rasmussen, A.F. and Lie, K.A. [2014] Discretization of flow diagnostics on stratigraphic and unstructured grids. In: *ECMOR XIV – 14th European Conference on the Mathematics of Oil Recovery, Catania, Sicily, Italy, 8-11 September 2014*. EAGE.

Sehbi, B.S., Kang, S., Datta-Gupta, A. and Lee, W.J. [2011] Optimizing fracture stages and completions in horizontal wells in tight gas reservoirs using drainage volume calculations. In: *Proceedings of the North American Unconventional Gas Conference and Exhibition*. 14-16 June 2011, The Woodlands, Texas, USA.

Shahvali, M., Mallison, B., Wei, K. and Gross, H. [2012] An alternative to streamlines for flow diagnostics on structured and unstructured grids. *SPE J.*, **17**(3), 768–778.

Shook, G.M. and Forsmann, J.H. [2005] Tracer Interpretation using Temporal Moments on a Spreadsheet. Tech. Rep. INL report 05-00400, Idaho National Laboratory.

Sorbie, K.S. [1991] *Polymer-improved oil recovery*. Springer Science & Business Media.

Thiele, M.R. [2005] Streamline simulation. In: *8th International Forum on Reservoir Simulation*. Stresa / Lago Maggiore, Italy.

Thiele, M.R. and Batycky, R.P. [2003] Water injection optimization using a streamline-based workflow. In: *Proceedings of the SPE Annual Technical Conference and Exhibition*. 5-8 October 2003, Denver, Colorado.

Wen, T., Thiele, M.R., Ciaurri, D.E., Aziz, K. and Ye, Y. [2014] Waterflood management using two-stage optimization with streamline simulation. *Comput. Geosci.*, **18**(3-4), 483–504.

Zhou, Y., Muggeridge, A.H., Berg, C.F. and King, P.R. [2015] Quantifying viscous cross-flow and its impact on tertiary polymer flooding in heterogeneous reservoirs. In: *IOR 2015-18th European Symposium on Improved Oil Recovery*.